DOI: 10.1002/chem.200500915

Fine Tuning of the Oxidation Locus, and Electron Transfer, in Nickel Complexes of Pro-Radical Ligands

Olaf Rotthaus,[a] Olivier Jarjayes,*[a] Fabrice Thomas,*[a] Christian Philouze,[a] Carlos Perez Del Valle,[a] Eric Saint-Aman,[b] and Jean-Louis Pierre[a]

Abstract: A large number of complexes of the first-row transition metals with non-innocent ligands has been characterized in the last few years. The localization of the oxidation site in such complexes can lead to discrepancies when electrons can be removed either from the metal center (leading to an $M^{(n+1)+}$ closed-shell ligand) or from the ligand (leading to an M^{n+} open-shell ligand). The influence of the ligand field on the oxidation site in square-planar nickel complexes of redox-active ligands is explored herein. The tetradentate ligands employed herein incorporate two di-*tert*-butylphenolate (pro-phenoxyl) moieties and one orthophenylenediamine spacer. The links between the spacer and both phenolates are either two imines ($[Ni(L^1)]$), two amidates ($[Ni(L^3)]^{2-}$), or one amidate and one imine ($[Ni(L^2)]^{-}$). The structure of each nickel(II) complex is presented. In the non-coordinating solvent CH_2Cl_2, the one-electron-oxidized forms are ligand–radical species with a contribution from a singly occupied d orbital of the nickel. In the presence of an exogenous ligand, such as pyridine, a Ni^{III} closed-shell ligand form is favored: axial ligation, which stabilizes the trivalent nickel in its octahedral geometry, induces an electron transfer from the metal(II) center to the radical ligand. The affinity of pyridine for the phenoxyl-nickel(II) species is correlated to the N-donor ability of the linkers.

Keywords: electron transfer · nickel · radicals · Schiff bases · tautomerism

Introduction

A fascinating class of metalloproteins use free radicals as cofactors to promote oxidation reactions.[1] Galactose oxidase, which belongs to this class, nicely illustrates the high degree of sophistication that can be reached in biocatalysis when a radical and a metal work in synergy. Several biomimetic approaches have been developed by chemists during the last decade to get insights into the metal–radical interaction. Consequently, a large number of complexes of the first-row transition metals with noninnocent ligands have been characterized.[2] These ligands, in their diamagnetic form, mainly incorporate phenoxyl or (imino)semiquinonate coordinating groups. With the aim of modeling the active site of galactose oxidase, we have recently prepared several phenoxyl copper(II) complexes.[3] In particular, we have shown that the phenolatocopper(II) complexes of H_2L^1 and other salen-type ligands can undergo a one-electron oxidation into magnetically interacting phenoxyl copper(II) complexes.[4,5] The localization of the oxidation site in such complexes could, however, lead to discrepancies as electrons can be removed either from the metal center (leading to an $M^{(n+1)+}$ closed-shell ligand) or from the ligand (leading to an M^{n+} open-shell ligand), and this situation could become even more complicated when valence tautomerism exists between these two forms, as in nickel porphyrins:[7] in this case, the two forms—the $M^{(n+1)+}$ closed-shell porphyrin and the M^{n+} open-shell porphyrin—are in equilibrium.

An understanding of the properties of such systems is of major interest not only from a theoretical point of view but also for the design of molecular electronic devices and switches.[8] This has, for example, recently stimulated the

[a] Dr. O. Rotthaus, Dr. O. Jarjayes, Dr. F. Thomas, Dr. C. Philouze, Dr. C. Perez Del Valle, Prof. Dr. J.-L. Pierre
Laboratoire de Chimie Biomimétique, LEDSS, UMR CNRS 5616
Université J. Fourier
BP 53, 38041, Grenoble Cedex 9 (France)
Fax: (+33) 4-7651-4836
E-mail: Olivier.Jarjayes@ujf-grenoble.fr
Fabrice.Thomas@ujf-grenoble.fr

[b] Prof. Dr. E. Saint-Aman
LEOPR, UMR CNRS 5630
Université J. Fourier, BP 53
38041 Grenoble Cedex 9 (France)

Supporting information for this article is available on the WWW under http://www.chemeurj.org/ or from the author.

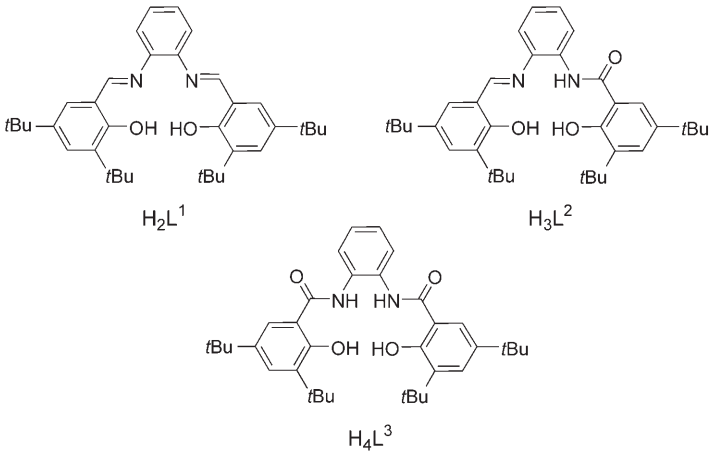

synthesis of nickel complexes with dioxolene ligands that exhibit such valence tautomerism.[9]

In slightly distorted square-planar nickel complexes, the energy levels of the potentially redox-active orbitals—π from the ligand or d from the metal—are very similar: by shifting one above the other (modulation of the ligand field), a metal-based or ligand-based redox process can be favored. With this goal, we present in this paper the one-electron oxidative chemistry of a series of nickel(II) complexes of pro-phenoxyl ligands possessing two di-*tert*-butylphenolates and two N-chelating groups: two imines for H_2L^1, one imine and one amidate for H_3L^2, and two amidates for H_4L^3. The ligand field is shown to dramatically affect the oxidation locus in these compounds.

Results and Discussion

Preparation of the ligands: H_2L^1 was obtained by condensation of *o*-phenylenediamine with 3,5-di-*tert*-butylbenzaldehyde. Coupling 3,5-di-*tert*-butylsalicyl chloride and 2-amino-1-(3,5-di-*tert*-butyl-2-hydroxybenzimino)benzene in CH_2Cl_2 affords H_3L^2. H_4L^3 was obtained by coupling *o*-phenylenediamine with 3,5-di-*tert*-butylsalicyl chloride.

Structures and spectroscopic properties of the nickel(II) complexes: The three ligands provide an N_2O_2 coordination sphere for a single nickel ion. Mixing one equivalent of $Ni(OAc)_2{\cdot}4H_2O$, two equivalents of NEt_3, and H_2L^1 in ethanol affords $[Ni(L^1)]$ (**1**). Similarly, the reaction of H_3L^2 with two equivalents of $Ni(OAc)_2{\cdot}4H_2O$ and four equivalents of NEt_3 (containing one equivalent of $nBu_4N^+OH^-$) in ethanol gave the low-spin complex $[Ni(L^3)]^-$ (**2**$^-$). $[Ni(L^3)]^{2-}$ (**3**$^{2-}$) was obtained by adding 1.2 equivalents of $Ni(OAc)_2{\cdot}4H_2O$ to H_4L^3 in DMF in the presence of four equivalents of $nBu_4N^+OH^-$.

The X-ray crystal structures (Table 1) of **1**, **2**$^-$, and **3**$^{2-}$ are depicted in Figures 1–3, respectively, and selected bond lengths and angles are reported in Table 2. The metal ion is coordinated to two imine or amidate nitrogens (N1, N2) and two phenolate oxygens (O1, O2). The N_2O_2Ni coordination polyhedron is essentially square planar but is slightly distorted towards tetrahedral.

Table 1. Crystallographic data for $[Ni(L^1)]$, $[Ni(L^2)]^-$, and $[Ni(L^3)]^{2-}$.

	$[Ni(L^1)]$	$[Ni(L^2)]^-$	$[Ni(L^3)]^{2-}$
formula	$C_{36}H_{46}N_2NiO_2$	$C_{42}H_{61}N_3NiO_3$	$C_{68}H_{116}N_4NiO_4$
M	597.47	714.66	1112.39
crystal system	triclinic	monoclinic	triclinic
space group	$P\bar{1}$	$P2_1/a$	$P\bar{1}$
a [Å]	9.190(2)	12.108(2)	13.753(4)
b [Å]	12.981(3)	26.330(5)	15.770(6)
c [Å]	14.386(4)	12.901(3)	16.969(7)
α [°]	107.98(2)	90	107.46(2)
β [°]	93.46(2)	95.59	110.33(3)
γ [°]	95.56(2)	90	80.06(3)
V [Å^3]	1617.3(8)	4093(1)	3282(3)
Z	2	4	2
T/K	150	293	150
ρ_{calcd} [g cm^{-3}]	1.227	1.160	1.125
μ [cm^{-1}]	6.33	5.13	3.43
monochromator	graphite	graphite	graphite
radiation	$Mo_{K\alpha}$	$Mo_{K\alpha}$	$Mo_{K\alpha}$
wavelength [Å]	0.71073	0.71073	0.71073
reflections collected	41422	14325	61054
independent reflections	9384	6515	16559
(R_{int})	(0.14400)	(0.06301)	(0.16874)
observed reflections	7811	4603	9191
	$[I>2\sigma(I)]$	$[I>2\sigma(I)]$	$[I>2\sigma(I)]$
R	0.0557	0.0538	0.0765
R_w	0.0786	0.0715	0.1125

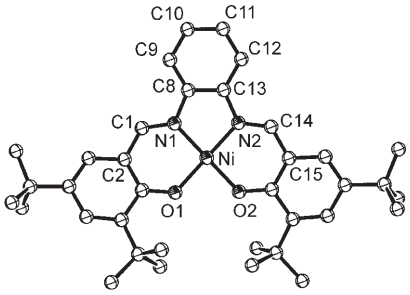

Figure 1. X-ray crystal structure of $[Ni(L^1)]$ (**1**) shown with 30% thermal ellipsoids.

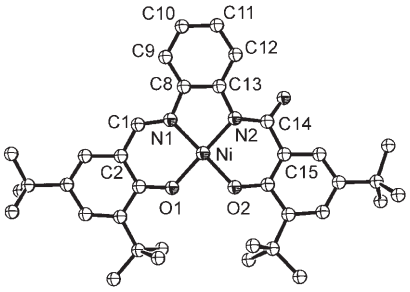

Figure 2. X-ray crystal structure of $[Ni(L^2)]^-$ (**2**) shown with 30% thermal ellipsoids.

The Ni–O1, Ni–O2, Ni–N1, and Ni–N2 bond lengths in **1** (Figure 1) are roughly similar (1.854(1), 1.850(1), 1.852(1) and 1.857(1) Å, respectively). This behavior contrasts with

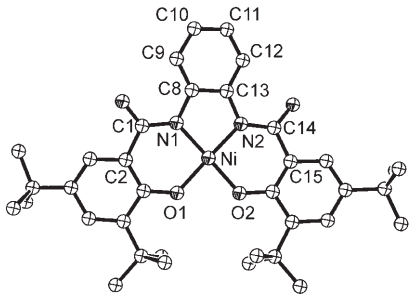

Figure 3. X-ray crystal structure of $[Ni(L^3)]^{2-}$ (**3**) shown with 30% thermal ellipsoids.

Table 2. Selected bond lengths [Å] and angles [°] for $[Ni(L^1)]$, $[Ni(L^2)]^-$, and $[Ni(L^3)]^{2-}$.

		$[Ni(L^1)]$			
Ni–O1	1.854(1)	Ni–O2	1.850(1)	Ni–N1	1.852(1)
Ni–N2	1.857(1)	O1–C3	1.303(2)	O2–C16	1.303(2)
C1–C2	1.420(2)	C1–N1	1.305(2)	C14–C15	1.419(3)
N2–C14	1.308(2)	O1-Ni-N1	94.6(1)	O2-Ni-N2	94.7(1)
O1-Ni-O2	85.9(1)	N1-Ni-N2	85.5(1)	O1-Ni-N2	174.7(1)
O2-Ni-N1	173.2(1)				
		$[Ni(L^2)]$			
Ni–O1	1.856(2)	Ni–O2	1.843(2)	Ni–N1	1.857(2)
Ni–N2	1.871(2)	O1–C3	1.301(4)	O2–C16	1.307(4)
C1–C2	1.422(5)	C1–N1	1.289(4)	C14–C15	1.479(4)
N2–C14	1.338(4)	O1-Ni-N1	93.8(1)	O2-Ni-N2	95.1(1)
O1-Ni-O2	85.1(1)	N1-Ni-N2	86.4(1)	O1-Ni-N2	173.8(1)
O2-Ni-N1	177.0(1)				
		$[Ni(L^3)]$			
Ni–O1	1.853(3)	Ni–O2	1.845(3)	Ni–N1	1.876(3)
Ni–N2	1.867(3)	O1–C3	1.310(5)	O2–C16	1.308(5)
C1–C2	1.491(5)	C1–N1	1.357(5)	C14–C15	1.493(5)
N2–C14	1.354(5)	O1-Ni-N1	95.4(1)	O2-Ni-N2	95.1(1)
O1-Ni-O2	83.3(1)	N1-Ni-N2	86.7(1)	O1-Ni-N2	175.4(1)
O2-Ni-N1	174.1(1)				

that of $[Cu(L^1)]$ (the nickel atom has been replaced by a copper ion),[10] which exhibits Cu–O1 and Cu–O2 bonds (1.895(2) and 1.894(2) Å, respectively) that are shorter than the Cu–N1 and Cu–N2 ones (1.941(2) and 1.945(2) Å, respectively). The mean deviation from the least-squares plane defined by the atoms N1, N2, O1, O2, and Ni is 0.0786 Å, with a dihedral angle between the O1-Ni-N1 and O2-Ni-N2 planes of 179°. The nitrogen atoms N1 and N2 are displaced 0.0903 and 0.0255 Å, respectively, from the plane defined by the atoms C8, C9, C10, C11, C12, and C13 (mean deviation of 0.0100 Å) and the torsion angle N1-C8-C13-N2 is 0.5°.

In the nickel complex $\mathbf{2}^-$ of the unsymmetrical tetradentate ligand H_3L^2 (Figure 2), the Ni–O1 and Ni–N1 distances of the salicylidene moiety (1.856(2) and 1.857(2) Å, respectively) are similar to those in **1**. The Ni–O2 and Ni–N2 distances in the *o*-hydroxybenzamidate moiety are 1.843(2) and 1.871(2), respectively. The mean deviation from the least-squares plane defined by the atoms N1, N2, O1, O2, and Ni is 0.058 Å, with a dihedral angle between the two O-Ni-N planes of 177°. The phenyl ring C8–C13 is more distorted than in **1**, as reflected by a mean deviation from the least-squares plane of 0.0147 Å. The N1 and N2 atoms are displaced 0.0987 and −0.0025 Å, respectively, from this plane, with a torsion angle around the N1-C8-C13-N2 bond of 0.9°.

The Ni–O1 and Ni–O2 bonds in $\mathbf{3}^{2-}$ (1.853(3) and 1.845(3) Å, respectively; Figure 3) are shorter than the Ni–N1 and Ni–N2 bonds (1.876(3) and 1.867(3) Å, respectively). The mean deviation from the least-squares plane defined by the atoms N1, N2, O1, O2, and Ni is 0.065 Å, a value that is intermediate between those of **1** and **2**. The dihedral angle between the two O–Ni–N planes is 179°, as for **1**. The phenyl ring C8–C13 deviates significantly from planarity (mean deviation of 0.0318 Å), with the nitrogen atoms N1 and N2 being displaced 0.2371 and −0.2218 Å, respectively, from this plane.

The UV/Vis spectrum of **1** in CH_2Cl_2 (Figure 4, Table 3) is dominated by intense absorptions at 383 ($\varepsilon = 29\,600\ M^{-1}cm^{-1}$), 470 (sh; $\varepsilon = 7000$), 492 ($\varepsilon = 9200$), and a low intensity shoulder at around 600 nm ($\varepsilon < 200$). The 490-nm band, which is absent in the optical spectrum of the free

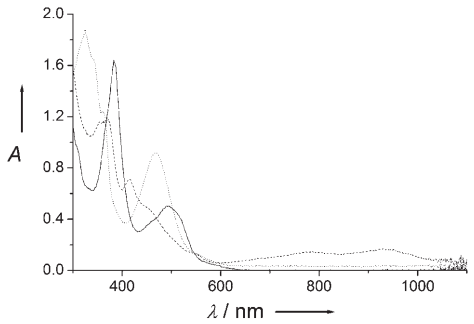

Figure 4. Electronic spectra of 0.05 mM solutions of $[Ni(L^1)]$ (solid lines) and electrogenerated $[Ni(L^1)]^+$ (dashed lines) in CH_2Cl_2 (+0.005 M TBAP). The dotted lines represent $[Ni(L^1)]^+$ in the presence of 5 mM pyridine. $T = 233$ K, $l = 1.000$ cm.

Table 3. Electronic properties of the nickel complexes in CH_2Cl_2 solution.

Complexes	λ_{max} [nm] (ε [$M^{-1}cm^{-1}$])[a]
$[Ni(L^1)]$	383 (29600), 492 (9200)
$[Ni(L^1)]^+$	370 (21700), 413 (12200), 458 sh (7560), 780 br (2420), 936 br (2480)
$[Ni(L^1)(Py)_2]^+$	325 (32200), 342 sh (28600), 362 sh (21500), 468 (16100)
$[Ni(L^1)]^{2+}$	375 (9620), 417 (9900), 445 (10000), 544 (3060), 918 (2900)
$[Ni(L^2)]^-$	325 (10600), 366 (10400), 427 (9400)
$[Ni(L^2)]$	345 sh (11600), 404 (9600), 432 (8600), 463 sh (6680), 922 br (2600)
$[Ni(L^2)(Py)_2]$	308 (20000), 433 (8600)
$[Ni(L^3)]^{2-}$	329 (17600), 374 (21400), 393 sh (17400), 501 (1000)
$[Ni(L^3)]^-$	342 (20000), 372 sh (15600), 414 sh (7600), 795 (2400)
$[Ni(L^3)(Py)_2]^-$	326 (30400), 457 (6400), 655 br (2800)
$[Ni(L^3)]$	337 (6100), 383 sh (4600), 476 (1600), 618 br (1600)

[a] UV/Vis spectra recorded at 233 K in the presence of 0.005 M TBAP (CH_2Cl_2 + 0.1 M TBAP solutions electrochemically oxidized and diluted twenty times); sh = shoulder, br = broad.

ligand, corresponds to a charge-transfer (CT) transition. As expected, this absorption is red-shifted (by 50 nm) and is less intense (by a factor of 2.5) than the CT transition of the previously described $[Cu(L^1)]$ complex.[5,10,11] The shorter-wavelength features are mainly associated with intraligand π–π* transitions, while the longer-wavelength bands correspond to d–d transitions.

The electronic spectrum of $\mathbf{2}^-$ (Figure 5, Table 3) exhibits absorptions at 325 ($\varepsilon = 10\,600\ M^{-1}cm^{-1}$), 366 ($\varepsilon = 10\,400$), 427 ($\varepsilon = 9400$), 500 (shoulder; $\varepsilon = 4000$), and 580 nm (shoulder;

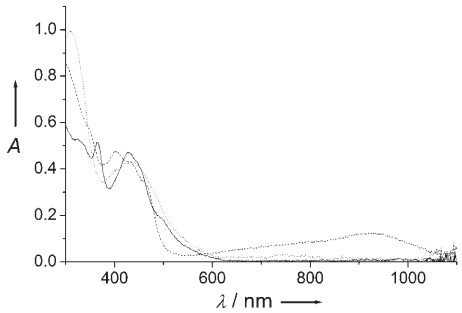

Figure 5. Electronic spectra of 0.05 mM solutions of $[Ni(L^2)]^-$ (solid lines) and electrogenerated $[Ni(L^2)]$ (dashed lines) in CH_2Cl_2 (+0.005 M TBAP). The dotted lines represent $[Ni(L^2)]$ in the presence of 5 mM pyridine. $T = 233$ K, $l = 1.000$ cm.

$\varepsilon = 500$) whose assignment is as follows: the higher-wavelength feature corresponds to d–d transitions, the CT transitions are observed in the 370–500 nm range, while the shorter-wavelength absorptions are attributed to intraligand π–π* transitions.

The visible spectrum of $[Ni(L^3)]^{2-}$ (Figure 6, Table 3) in CH_2Cl_2 reveals transitions at 329 (shoulder; $\varepsilon = 17\,600\ M^{-1}cm^{-1}$), 374 ($\varepsilon = 21\,400$), 501 ($\varepsilon = 1000$), and 550 nm (shoulder; $\varepsilon = 400$). The two latter bands are attributed to d–d transitions, while the former correspond to π–π* and CT transitions. Similar transitions are found in the UV/Vis spectra of **1**, $\mathbf{2}^-$, and $\mathbf{3}^{2-}$ in CH_3OH (Table 4).

Electrochemistry of the nickel(II) complexes: The electrochemical behavior of the nickel complexes was studied in CH_2Cl_2 and CH_3OH (with 0.1 M TBAP as supporting elec-

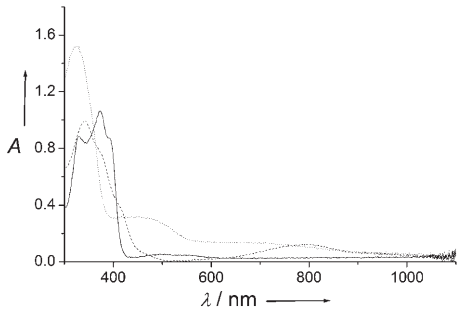

Figure 6. Electronic spectra of 0.05 mM solutions of $[Ni(L^3)]^{2-}$ (solid lines) and electrogenerated $[Ni(L^3)]^-$ (dashed lines) in CH_2Cl_2 (+0.005 M TBAP). The dotted lines represent $[Ni(L^3)]^-$ in the presence of 25 mM pyridine. $T = 233$ K, $l = 1.000$ cm.

trolyte) by cyclic voltammetry (CV), differential pulse voltammetry (DPV), and rotating disc electrode (RDE) voltammetry. All potentials are referenced to the ferrocenium/ferrocene couple.

In CH_2Cl_2, the CV curves of **1** and $\mathbf{2}^-$ (Figure 7, Table 5) exhibit two reversible redox waves (at $E_{1/2}{}^1 = 0.582$, $E_{1/2}{}^2 = 0.802$ V and $E_{1/2}{}^1 = 0.150$, $E_{1/2}{}^2 = 0.806$ V versus Fc^+/Fc for

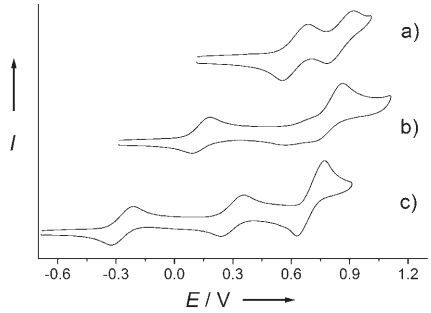

Figure 7. CV curves of 1 mM CH_2Cl_2 solutions (+0.1 M TBAP) of: a) $[Ni(L^1)]$, b) $[Ni(L^2)]^-$, and c) $[Ni(L^3)]^{2-}$. Scan rate: 0.1 $V s^{-1}$; $T = 298$ K. The potentials are referenced against Fc^+/Fc.

$[Ni(L^1)]$ (**1**) and $[Ni(L^2)]^-$ ($\mathbf{2}^-$), respectively), while three waves are observed for $[Ni(L^3)]^{2-}$ ($\mathbf{3}^{2-}$; at $E_{1/2}{}^1 = -0.254$, $E_{1/2}{}^2 = 0.306$, and $E_{1/2}{}^3 = 0.706$ V versus Fc^+/Fc). All of these correspond to one-electron processes, as judged by coulometry and RDE voltammetry. The $E_{1/2}{}^1$ oxidation potentials are remarkably dependent on the coordinating nitrogens, and thus on the global charge of the complex: the higher value is observed for **1** (two imines), the lower for $\mathbf{3}^{2-}$ (two amidates), while an intermediate potential is obtained for $\mathbf{2}^-$. In the presence of pyridine, the $E_{1/2}{}^1$ and $E_{1/2}{}^2$ values are shifted towards

Table 4. Spectroscopic properties of nickel complexes in MeOH solution.

Complexes	λ_{max} [nm] (ε [$M^{-1}cm^{-1}$])[a]
$[Ni(L^1)]$	381 (29 800), 486 (9600)
$[Ni(L^1)]^+$	317 (29 800), 334 sh (25 500), 355 sh (21 300), 460 (14 400)
$[Ni(L^1)(Py)_2]^+$	317 (27 700), 334 sh (24 500), 356 sh (19 700), 457 (13 300)
$[Ni(L^1)]^{2+}$	314 (17 600), 446 (6800), 930 br (800)
$[Ni(L^2)]^-$	321 (10 800), 370 (9600), 408 (8200), 481 (3800)
$[Ni(L^2)]$	313 (20 800), 432 (9000)
$[Ni(L^2)(Py)_2]$	306 (21 000), 411 (8600)
$[Ni(L^3)]^{2-}$	334 (13 600), 363 (11 400), 388 sh (8200), 515 (600)
$[Ni(L^3)]^-$	327 (15 400), 361 sh (10 800), 821 (2600)
$[Ni(L^3)(Py)_2]^-$	316 (18 800), 466 (2800), 645 br (1000)

[a] UV/Vis spectra recorded at 233 K in the presence of 0.005 M TBAP (CH_2Cl_2 + 0.1 M TBAP solutions electrochemically oxidized and diluted twenty times); sh = shoulder, br = broad.

Table 5. Redox properties of the nickel complexes

Complex	Solvent	$E_{1/2}$ [V][a]		
$[Ni(L^1)]$	CH_2Cl_2	0.582	0.802	
	CH_2Cl_2 + 5 equiv of Py	0.574	0.758	
	MeOH	0.466	0.670	
$[Ni(L^2)]^-$	CH_2Cl_2	0.150	0.806	
	CH_2Cl_2 + 50 equiv of Py	0.102	0.61	
	MeOH	0.234	0.514	
$[Ni(L^3)]^{2-}$	CH_2Cl_2	−0.254	0.306	0.706
	CH_2Cl_2 + 1000 equiv of Py	−0.322	0.074	0.626
	MeOH	−0.054	0.290	

[a] Potential values given relative to the Fc/Fc^+ reference electrode, T = 298 K, complex concentrations are 1 mM. $E_{1/2}$ values were obtained from DPV measurements by adding half of the pulse amplitude to the E_p value. The confidence level is ±0.005 V.

the cathodic region, which suggests that the oxidized forms are stabilized in the presence of an exogenous N-donor ligand (Table 5).

The CV curves of **1**, $\mathbf{2}^-$, and $\mathbf{3}^{2-}$ in the coordinating solvent CH_3OH show waves that are less reversible than those obtained in CH_2Cl_2; the oxidation potentials are slightly displaced. A cathodic shift of $E_{1/2}{}^1$ is observed for the Schiff-base complex **1**, while it is anodic for $\mathbf{2}^-$ and $\mathbf{3}^{2-}$: there is therefore no simple correlation between $E_{1/2}{}^1$ and the structure of the complex in CH_3OH.

One-electron-oxidized complexes in CH_2Cl_2: The one-electron-oxidized complexes $\mathbf{1}^+$, **2**, and $\mathbf{3}^-$ were generated electrochemically in CH_2Cl_2 (with 0.1 M TBAP as supporting electrolyte) at 233 K under argon.

The electronic spectra of $\mathbf{1}^+$, **2**, and $\mathbf{3}^-$ exhibit remarkable bands in the 800–1000 nm region (Figures 4–6). Based on their high intensity ($1000 < \varepsilon < 3400\ M^{-1}cm^{-1}$), they correspond to CT transitions. Similar bands, although less intense, were observed in the phenoxyl radical complex $[Cu(L^1)]^+$.[5] Additional features are observed in the 400–450 nm region, where the π–π* transitions of phenoxyl radicals are expected to be found.[12] These data thus suggest a ligand-centered, rather than metal-centered, oxidation process at 233 K. The one-electron-oxidized species are highly stable in solution at 298 K, with less than 5% degradation within 10 h for $\mathbf{1}^+$ and **2** and less than 3% degradation within six days for $\mathbf{3}^-$.

The X-band EPR spectrum of $\mathbf{1}^+$ at 260 K in CH_2Cl_2 (+0.1 M TBAP) exhibits an isotropic and unresolved ($S = 1/2$) signal centered at $g_{iso} = 2.034$ (peak-to-peak line width of 3.1 mT, Figure 8). This g_{iso} value is intermediate between that obtained for the phenoxyl zinc(II) analogue $[Zn(L^1)]^+$[13] and that of typical Ni^{III} complexes (roughly 2.13–2.17).[14] $\mathbf{1}^+$ is thus best formulated as a ligand radical, with partial delocalization of the unpaired electron onto the orbitals of the nickel atom. The EPR spectrum of $\mathbf{1}^+$ in CH_2Cl_2 (+0.1 M TBAP) at 100 K contrasts sharply with that recorded at 260 K. It consists of a rhombic ($S = 1/2$) signal, with g values at 2.270, 2.220, and 2.022 ($g_{av} = 2.17$) that are typical of Ni^{III} complexes in a low-spin configuration. The pattern of g values ($g_x \approx g_y > g_z \approx g_e$) is indicative of a d_{z^2} ground state where the z-axis is perpendicular to the plane of the molecule. The temperature-dependence of the EPR spectra of $\mathbf{1}^+$ shows that the change of shape (Ni^{III} to radical) occurs at around 170–190 K, which is the melting point of the solvent.[15] A similar behavior has recently been reported by Yamauchi et al. and interpreted as a valence tautomerism governed by the temperature.[16] An alternative explanation could be relaxation effects: as the metal relaxes faster than the radical, only the radical contribution is detected in liquid CH_2Cl_2. Because none of these arguments is particularly strong, we still entertain both possibilities.

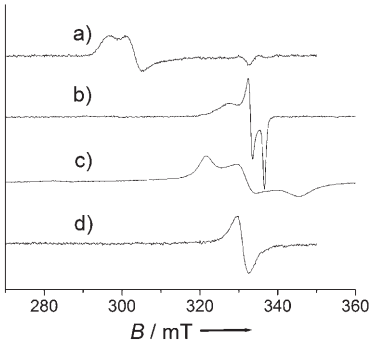

Figure 8. X-band EPR spectra of CH_2Cl_2 solutions (+0.1 M TBAP) of: a) 1 mM $[Ni(L^1)]^+$ at 100 K, b) 10 mM $[Ni(L^2)]$ at 100 K, c) 1 mM $[Ni(L^3)]^-$ at 100 K, and d) 1 mM $[Ni(L^1)]^+$ at 260 K. Microwave frequency: 9.42 GHz; power: 20 mW; modulation frequency: 100 kHz; amplitude: 0.4 mT.

Both **2** and $\mathbf{3}^-$ are EPR-silent at 233 K,[17] although lowering the temperature to 100 K results in the appearance of a rhombic ($S = 1/2$) signal (Figure 8, Table 6), with a moderate g-tensor anisotropy ($g = 2.09$, 2.03, 1.95 and 2.048, 2.020, 1.999 for $[Ni(L^2)]$ and $[Ni(L^3)]^-$, respectively) and g_{av} values of 2.022 and 2.015, respectively. These are lower than any reported for Ni^{III} complexes[14] or high-spin nickel(II) magnetically coupled to a radical.[18] On the other hand, both the g_{av} values and the g-tensor anisotropy are higher than those of phenoxyl radicals, thus suggesting that **2** and $\mathbf{3}^-$ are ligand radicals with contribution from the singly occupied d orbital of Ni^{III}.[19] The EPR spectrum of **2** does not match either that of $\mathbf{1}^+$ (i.e., a salicylidene(phenoxyl)nickel complex) or that of $\mathbf{3}^-$ (i.e., an *o*-hydroxybenzamidate-(phenoxyl)nickel complex), which suggests a contribution from the two resonance structures shown in Scheme 1 to the electronic distribution in $\mathbf{1}^+$, **2**, and $\mathbf{3}^-$. These results were confirmed by DFT calculations on $\mathbf{3}^-$ performed at the B3LYP level (Figure 9): the calculated SOMO is mainly developed on the ligand, with contribution of a nickel d_{xy}, d_{xz}, or d_{yz} orbital. As expected, the ligand SOMO is equally developed on both phenoxyl moieties, thus indicating the delocalization of the unpaired electron as depicted in Scheme 1.

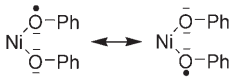

Scheme 1. Resonance structures for $[Ni(L^3)]^-$.

The three complexes $\mathbf{1}^+$, **2**, and $\mathbf{3}^-$ thus exhibit a ligand radical character, with contribution of a nickel orbital.

Table 6. EPR parameters of the one-electron-oxidized nickel complexes.

Complex	Solvent[a]	g values				A values		
		g_{xx}	g_{yy}	g_{zz}	g_{av}	A_{xx}	A_{yy}	A_{zz}
$[Ni(L^1)]^+$	CH_2Cl_2	2.270	2.220	2.022	2.171			
	CH_2Cl_2+Py[b]	2.200	2.168	2.027	2.132	1.65	1.65	2.14
	MeOH	2.287	2.228	2.023	2.179			
	MeOH+Py[b]	2.205	2.170	2.026	2.134	1.65	1.65	2.14
$[Ni(L^2)]$	CH_2Cl_2	2.048	2.020	1.999	2.022			
	CH_2Cl_2+Py[b]	2.218	2.181	2.026	2.142	1.60	1.55	2.10
	MeOH	2.309	2.246	2.020	2.192			
	MeOH+Py[b]	2.218	2.183	2.027	2.143	1.55	1.55	2.10
$[Ni(L^3)]^-$	CH_2Cl_2	2.086	2.017	1.941	2.015			
	CH_2Cl_2+Py[b]	2.227	2.203	2.024	2.151	1.55	1.55	2.04
	MeOH	2.328	2.270	2.018	2.205			
	MeOH+Py[b]	2.223	2.195	2.024	2.147	1.55	1.55	2.04

[a] At 100 K in the presence of 0.1 M TBAP. [b] 0.1 M pyridine.

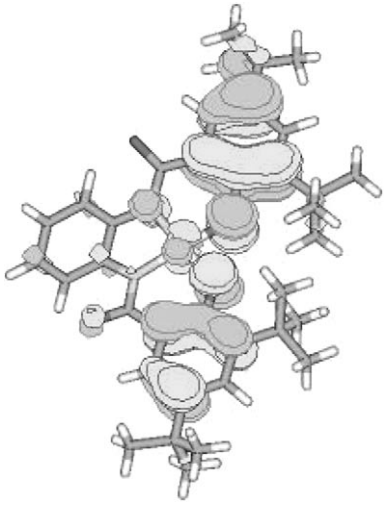

Figure 9. Optimized structure and calculated SOMO for $[Ni(L^3)]^-$. Calculations performed at the B3LYP level using the Lanl2dz basis set.

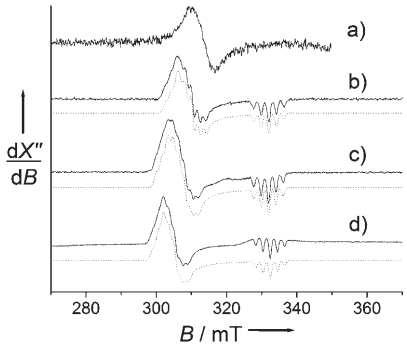

Figure 10. X-band EPR spectra of 1 mM CH_2Cl_2 solutions (+0.1 M TBAP + 5000 equivalents of pyridine) of: a) $[Ni(L^1)]^+$ at 233 K, b) $[Ni(L^1)]^+$ at 100 K, c) $[Ni(L^2)]$ at 100 K, and d) $[Ni(L^3)]^-$ at 100 K. Solid lines represent experimental spectra and dotted lines are simulations using the parameters given in Table 6. Microwave frequency: 9.42 GHz; power: 20 mW; modulated frequency: 100 kHz; amplitude 0.1 mT.

One-electron-oxidized complexes in CH_2Cl_2/pyridine and CH_3OH: Increasing amounts of pyridine were added to CH_2Cl_2 solutions of the radical complexes $\mathbf{1}^+$, **2**, and $\mathbf{3}^-$ at 298 K and dramatic color changes were observed: the orange solution of $\mathbf{1}^+$ turns brown, as do the green solutions of **2** and $\mathbf{3}^-$. The evolution of the electronic spectra during titration follows a similar trend, namely the disappearance of the 900–1000-nm absorption.

For $\mathbf{1}^+$, a broad absorption, assigned to Ni^{III} d–d transitions, appears around 700–900 nm, whereas the shorter-wavelength absorption at around 400–600 nm is attributed to CT transitions. This Ni^{III}, rather than ligand radical, state was confirmed by EPR spectroscopy at 298 K, which reveals an isotropic ($S=1/2$) signal centered at a g_{iso} value of 2.15 (Figure 10a).[14]

No other absorptions could be observed above 600 nm in the electronic spectrum of **2** in the presence of pyridine, although medium-intensity bands, attributed to CT, are present at 560 (shoulder; $\varepsilon=2340\ M^{-1}cm^{-1}$) and 468 nm ($\varepsilon=18460$). Similarly, the visible spectrum of $\mathbf{3}^-$ in the presence of 10000 equivalents of pyridine exhibits Ni^{III} d–d transitions at wavelengths higher than 600 nm and medium-intensity CT transitions in the range 400–600 nm (Table 3).

Among the surveyed compounds, $\mathbf{3}^-$ has the lowest affinity for pyridine, with a $\log\beta$ value at 298 K for the equilibrium shown in Equation (1) of only $2.41\pm0.06\ M^{-2}$; $\log\beta$ is $6.71\pm0.09\ M^{-2}$ for $\mathbf{1}^+$.[20] The stronger donor capacity of the amido N-donors thus lowers the affinity of the complexes for axial ligands.[21]

$$[Ni(L)] + 2\,Py \rightleftharpoons [Ni(L)(Py)_2]\ \beta = [Ni(L)(Py)_2]/([Ni(L)] \times [Py]^2) \quad (1)$$

Lowering the temperature from 298 to 233 K results in an increase of $\log\beta$ by three units for $\mathbf{3}^-$ and two units for $\mathbf{1}^+$. As the color of the pyridine adduct is different from that of the radical complex, a thermochromism is observed for $\mathbf{1}^+$ and $\mathbf{3}^-$ in the presence of one and 100 equivalents of pyridine, respectively. This thermochromism is more marked for $\mathbf{3}^-$ than for $\mathbf{1}^+$, in agreement with the difference of $\log\beta$ (see Supporting Information).

The EPR spectra of the pyridine adducts of $\mathbf{1}^+$, **2**, and $\mathbf{3}^-$ in CH_2Cl_2 at 100 K are shown in Figure 10. A low-spin ($S=1/2$) Ni^{III} signal, with hyperfine splitting in each of the three g components, is systematically observed. The pattern of g values is consistent with an octahedral geometry around the metal. In addition, the presence of one well-resolved quintuplet in the high-field component, as well as two less-resolved quintuplets in the low-field component, implies the existence of the six-coordinate Ni^{III} adducts $[Ni(L^1)(Py)_2]^+$ ($\mathbf{4}^+$), $[Ni(L^2)(Py)_2]$ (**5**), and $[Ni(L^3)(Py)_2]^-$ ($\mathbf{6}^-$) with two equivalent pyridines axially bonded ($2\times 2I_N+1$ transitions; $I_N=1$).[22] Replacement of the imine nitrogens by amidate induces both a lowering of A_{zz} and an increase of g_{xx} and g_{yy} due to a weakening of the axial bonds.[23] This explanation is consistent with the measured pyridine binding, which follows the order $\mathbf{1}^+ > \mathbf{2} > \mathbf{3}^-$.

The electronic spectra of the oxidized species $\mathbf{1}^+$ are roughly similar in CH_3OH and CH_2Cl_2/pyridine. The same behavior is observed for **2**, which suggests that the oxidation products in CH_3OH contain Ni^{III}. Addition of pyridine to the one-electron-oxidized complexes $\mathbf{1}^+$ and **2** in CH_3OH does not induce significant changes in their visible spectra, thus confirming that these species are already octahedral Ni^{III} complexes with two solvent molecules bound axially. However, $\mathbf{3}^-$ exhibits a quite different behavior: the oxidized product in CH_3OH at 233 K exhibits strong absorptions at 821 ($\varepsilon = 2600\ M^{-1}cm^{-1}$) and 327 nm ($\varepsilon = 15400$) and unresolved bands in the region 350–500 nm. These bands, which match reasonably well with those observed in neat CH_2Cl_2 for the radical complex, disappear upon addition of excess pyridine to give a more typical octahedral Ni^{III} spectrum. $\mathbf{3}^-$ thus has a radical character both in CH_2Cl_2 and CH_3OH. Conversion of this radical species into the corresponding Ni^{III} complex requires a strong N-donor exogenous ligand (CH_3OH is known to have only a moderate coordinating ability).

The EPR spectra of the one-electron-oxidized complexes $\mathbf{1}^+$, **2**, and $\mathbf{3}^-$ in CH_3OH at 100 K, in the absence of pyridine, show rhombic low-spin Ni^{III} signals. The geometry around the metal center is expected to be similar to that in the mixture of CH_2Cl_2 and pyridine since the pattern of g values is similar. As expected, no hyperfine coupling could be detected in any of the g component (the ^{16}O isotope has no nuclear spin). The g_x and g_y values obtained for the CH_3OH adduct are higher than those measured for the pyridine adduct, which reflects a stronger interaction between the metal d_{z^2} orbital and the axial pyridine lone-pair that destabilizes the nickel SOMO.[23]

Ni^{III} species are thus systematically observed in the mixture of CH_2Cl_2 and pyridine, while delocalized radicals are observed in CH_2Cl_2 alone. Axial ligation of pyridine shifts the d_{z^2} orbital above the filled ligand orbitals and promotes an electron transfer from the metal to the open-shell ligand.

Both $\mathbf{1}^+$ and **2** have a Ni^{III} character in the coordinating solvent CH_3OH, which can be explained by axial ligation of two solvent molecules in a similar manner to pyridine. In contrast, $\mathbf{3}^-$ exhibits an EPR spectrum corresponding to an octahedral Ni^{III} moiety at 100 K (with two CH_3OH molecules axially bonded), and a radical UV/Vis spectrum at 233 K, similar to $\mathbf{1}^+$ in CH_2Cl_2. This may be explained by the weaker donor ability of CH_3OH (compared to pyridine) and the lower affinity of axial ligands for this complex, which does not favor an octahedral geometry.

Conclusion

The three ligands H_2L^1, H_3L^2, and H_4L^3 afford the slightly distorted square-planar nickel(II) complexes **1**, $\mathbf{2}^-$, and $\mathbf{3}^{2-}$, respectively, if no exogenous ligands are present. The corresponding one-electron-oxidized[24] species in CH_2Cl_2 are highly stable delocalized radicals with a contribution from the nickel orbital. Strong amido N-donors, which are known to stabilize high-valent metals, do not promote a simple metal-centered oxidation process. The energy levels of the potentially redox-active orbitals—π from the ligand, or d from the metal—thus remain almost the same in **2** and $\mathbf{3}^-$, as seen by the respective EPR spectra at 100 K (complex $\mathbf{1}^+$, which contains imino N-donors, exhibits a more marked nickel(III) character). The shift of one orbital above the other, that is, an intramolecular electron transfer (valence tautomerism), can be promoted by changing the geometry (from square planar to octahedral) around the metal center. The corresponding one-electron-oxidized complexes are nickel(III) phenolate complexes.

It has recently been shown[9] that the square-planar nickel(II) complex $[Ni^{II}(MePy(Bz)_2)(t\mathrm{Bu}_2\mathrm{Cat})]^-$ ($MePy(Bz)_2$ = *N*,*N*-bis(benzyl)-*N*-[(6-methyl-2-pyridyl)methyl]amine; $t\mathrm{Bu}_2\mathrm{Cat}$ = 3,5-di-*tert*-butylcatecholate) can be oxidized in a one-electron process, in CH_2Cl_2, into a nickel(III) catecholate species (**7**), which is converted into the nickel(II) radical complex **8** (Scheme 2) in the presence of exogenous ligands. This behavior contrasts sharply with that observed for $\mathbf{1}^+$, **2**, and $\mathbf{3}^-$ where, upon addition of strong exogenous ligands, the delocalized radical species are converted into nickel(III) phenolate complexes. In these compounds, the nickel(III) ion resides in an octahedral geometry, with two pyridines bound axially (Scheme 2).

These results illustrate the high level of control of the oxidation locus that can be reached simply by modulating the ligand field. In addition, we have shown how it tunes the stability of the radical species, as well as its affinity for exogenous ligands.

Experimental Section

General: All chemicals were of reagent grade and were used without purification. Microanalyses were performed by the Service Central d'Analyses du CNRS (Lyon, France).

NMR spectra were recorded with a Bruker AM 300 spectrometer (^1H at 300 MHz, ^{13}C at 75 MHz). Chemical shifts are given relative to tetramethylsilane (TMS). Mass spectra were recorded with a Thermofunnigen (EI/DCI) apparatus.

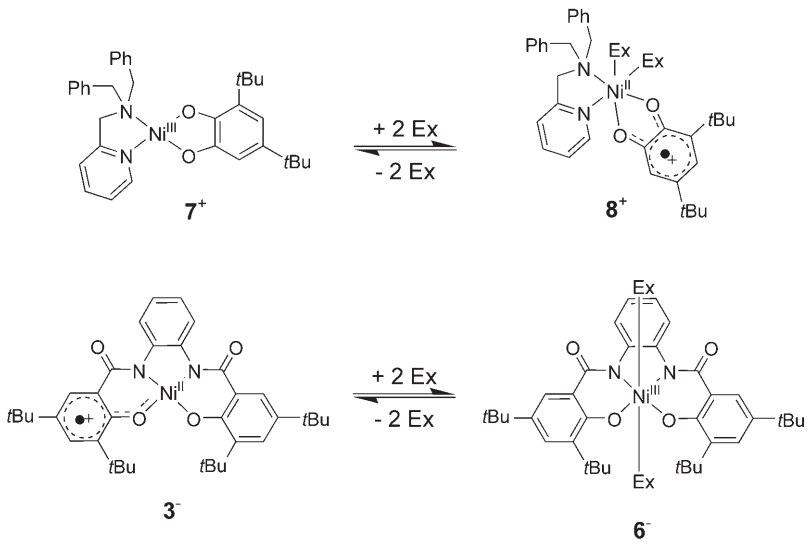

Scheme 2. Modulation of the oxidation locus by coordination of an exogenous ligand (Ex) to $\mathbf{3}^-$ (this work) and **7** (reference [9]).

UV/Vis spectroscopy: UV/Vis spectra were recorded at 298 K with a Perkin–Elmer Lambda 2 spectrophotometer equipped with a temperature controller unit set at 298 K. The path length of the quartz cell was 1.000 cm. Low-temperature visible spectra were recorded with a Cary 50 spectrophotometer equipped with a Hellma low-temperature immersion probe (1.000-cm path-length quartz cell).

The affinity constants were obtained by refinement of the UV/Vis titration data of the complexes with pyridine in CH_2Cl_2. The fit was performed with the commercial SPECFIT software according to Equation (1).

EPR spectroscopy: X-band EPR spectra were recorded with a Bruker ESP 300E spectrometer equipped with a Bruker nitrogen-flow cryostat. Spectra were treated by using the WINEPR software and simulated using the Bruker SIMFONIA software. Spectra were recorded at 100 K with 200-μL samples, while variable-temperature experiments were performed with 50-μL samples.

Electrochemistry: The cyclic and differential pulse voltammograms of each compound (1 mM) in CH_2Cl_2 containing 0.1 M tetra-*n*-butylammonium perchlorate (TBAP) as supporting electrolyte were recorded with a CHI 660 potentiostat at 298 K using a glassy carbon disc as working electrode, a Pt wire as secondary electrode, and an $Ag/AgNO_3$ (0.01 M) reference electrode. The potential of the ferrocenium/ferrocene (Fc^+/Fc) couple was used as an internal reference (+0.087 V under our experimental conditions). Experiments were performed under argon. Electrolysis at a carbon-felt electrode was performed at 233 K, by controlled potential electrolysis, with a PAR 273 potentiostat. It was followed by rotating disc voltammetry (carbon-disc electrode, 600 rpm).

Crystal structure analysis: For all structures, the collected reflections were corrected for Lorentz and polarization effects but not for absorption. The structures were solved by direct methods and refined by using the teXsan software package (texsan, Crystal Structure Analysis Package, Molecular Structure, Corp., The Woodlands, TX, **1992**). All non-hydrogen atoms were refined with anisotropic thermal parameters. Hydrogen atoms were generated in idealized positions, riding on the carrier atoms, with isotropic thermal parameters. CCDC-269657 ($[Ni(L^1)]$), CCDC-269762 ($[Ni(L^2)]^-$), and CCDC-269450 ($[Ni(L^3)]^{2-}$) contain the supplementary crystallographic data for this paper. These data can be obtained free of charge from the Cambridge Crystallographic Data Centre via www.ccdc.cam.ac.uk/data_request/cif.

Preparation of the ligands and complexes

1,2-Bis(3,5-di-*tert*-butyl-2-hydroxybenzimino)benzene (H_2L^1): H_2L^1 was prepared by refluxing *o*-phenylenediamine (one equivalent) and 3,5-*tert*-butyl-2-hydroxybenzaldehyde (two equivalents) in ethanol according to the procedure published by Wöltinger et al.[25]

3,5-Di-*tert*-butylsalicyl chloride: 3,5-Di-*tert*-butylsalicylic acid hydrate (1.0 g, 4 mmol) was dissolved in THF (50 mL). Thionyl chloride (5.9 mL, 80 mmol) was slowly added under nitrogen, while cooling in an ice bath, and the mixture was stirred overnight and then allowed to warm to room temperature. The solvent and the excess thionyl chloride were evaporated in vacuo and the resulting product, isolated as a pale-yellow oil, was used directly in the next step without further purification. ^{1}H NMR (300 MHz, $CDCl_3$, 298 K, TMS): $\delta = 10.24$ (s, 1H), 7.91 (d, $^4J = 2.3$ Hz, 1H), 7.66 (d, $^4J = 2.3$ Hz, 1H), 1.42 (s, 9H), 1.33 ppm (s, 9H).

2-Amino-1-(3,5-di-*tert*-butyl-2-hydroxybenzimino)benzene: This precursor for H_3L^2 was prepared according to the procedure of Atwood et al.[26]

2-(3,5-Di-*tert*-butyl-2-hydroxybenzamido)-1-(3,5-di-*tert*-butyl-2-hydroxybenzimino)benzene (H_3L^2): As described below for the synthesis of ligand H_4L^3, 3,5-di-*tert*-butylsalicyl chloride (410 mg, 1.5 mmol) in dichloromethane (20 mL) was coupled with 2-amino-1-(3,5-di-*tert*-butyl-2-hydroxybenzimino)benzene (500 mg, 1.5 mmol) in dichloromethane (30 mL) and worked up in the same way. The raw product was purified by column chromatography over silica gel (100 g) with pentane/dichloromethane (1:1) to yield H_3L^2 as a beige powder (340 mg, 41%). ^{1}H NMR (300 MHz, $CDCl_3$, 298 K, TMS): $\delta = 12.43$ (br. s, 1H), 12.27 (s, 1H), 8.57 (s, 1H), 8.51 (s, 1H), 8.31 (dd, $^3J = 8.1$, $^4J = 1.1$ Hz, 1H), 7.43–7.41 (m, 2H), 7.3–7.0 (m, 5H), 1.36 (s, 9H), 1.35 (s, 9H), 1.25 (s, 9H), 1.19 ppm (s, 9H); UV/Vis (CH_2Cl_2): λ_{max} (ε) = 328 nm (18980 $M^{-1}cm^{-1}$); IR (neat): $\tilde{\nu}$ = 3476 w (ν_{OH}), 3427 (ν_{NH}), 2960, 2904, 2866 w (ν_{CH}), 1646 ($\nu_{C=O}$), 1616, 1586 ($\nu_{C=N}$) cm^{-1}; MS: *m/z* (%): 557 (100) $[M+H]^+$.

1,2-Bis(3,5-di-*tert*-butyl-2-hydroxybenzamido)benzene (H_4L^3): *o*-Phenylenediamine (220 mg, 2 mmol) was dissolved in dry dichloromethane (20 mL) and the solution was cooled to −40 °C. A solution of freshly prepared 3,5-di-*tert*-butylsalicyl chloride (ca. 4 mmol) in dry dichloromethane (50 mL) was then added dropwise to the cooled solution of the diamine, under nitrogen, then the cooling bath was removed and the mixture was stirred for a further two hours while it was allowed to warm to room temperature. The mixture was then filtered to remove a small amount of a white precipitate, washed with water (2 × 20 mL) and saturated NaCl solution (20 mL), and dried with sodium sulfate. The solvent was evaporated and the raw product recrystallized from methanol to yield H_4L^3 as a white powder (0.45 g, 40%). ^{1}H NMR (300 MHz, $CDCl_3$, 298 K, TMS): $\delta = 7.56$ (dd, $^3J = 6.0$, $^4J = 3.5$ Hz, 2H), 7.51 (d, $^4J = 2.2$ Hz, 2H), 7.38 (d, $^4J = 2.2$ Hz, 2H), 7.30 (dd, $^3J = 6.0$, $^4J = 3.5$ Hz, 2H), 1,43 (s, 18H), 1,28 ppm (s, 18H); UV/Vis (CH_2Cl_2): λ_{max} (ε) = 324 nm (12320 $M^{-1}cm^{-1}$); IR (neat): $\tilde{\nu}$ = 3428 w (ν_{OH}), 3303 (ν_{NH}), 2957, 2908, 2870 w (ν_{CH}), 1624 ($\nu_{C=O}$) cm^{-1}; MS: *m/z* (%): 573 (100) $[M+H]^+$.

$[Ni(L^1)]$: H_2L^1 (50 mg, 90 μmol) was dissolved in ethanol (40 mL) and a solution of $Ni(OAc)_2 \cdot 4H_2O$ (45 mg, 180 μmol) in ethanol (30 mL) was added, followed by triethylamine (26 μL, 180 μmol). The mixture was refluxed for three hours, then two thirds of the solvent was evaporated and the solution stored at −20 °C overnight. $[Ni(L^1)]$ (44 mg, 80%) was filtered off as fine, red needles and washed with ice-cold ethanol. Elemental analysis calcd (%) for $C_{36}H_{46}N_2NiO_2$: C 72.37, H 7.76, N 4.69, Ni 9.82; found: C 71.98, H 7.72, N 4.61, Ni 9.50; ^{1}H NMR (300 MHz, CD_2Cl_2, 298 K, TMS): $\delta = 8.33$ (s, 2H), 7.78 (dd, $^3J = 6.3$, $^4J = 3.3$ Hz, 2H), 7.46 (d, $^4J = 2.6$ Hz, 2H), 7.27 (dd, $^3J = 6.3$, $^4J = 3.3$ Hz, 2H), 7.20 (d, $^4J = 2.6$ Hz, 2H), 1,49 (s, 18H), 1,36 ppm (s, 18H); UV/Vis (CH_2Cl_2): λ_{max} (ε) =

383 nm (29600 $M^{-1}cm^{-1}$), 492 (9200); IR (neat): $\tilde{\nu}$ = 2959, 2897, 2864 w (ν_{CH}), and 1616, 1605, 1583 s ($\nu_{C=N}$) cm^{-1}. MS: *m/z* (%): 597 (100) $[M+H]^+$.

[Ni(L^2)](Bu$_4$N): Ni(OAc)$_2$·4H$_2$O (45 mg, 180 μmol) in ethanol (30 mL) was added to a solution of H_3L^2 (50 mg, 90 μmol) in ethanol (20 mL). After further addition of triethylamine (50 μL, 360 μmol) and Bu$_4$NOH (90 μL of a 1 M solution in methanol, 90 μmol), the mixture was refluxed for four hours. Two thirds of the solvent was then evaporated and, after storage overnight at −20 °C, [Ni(L^2)](Bu$_4$N) was obtained as a dark-orange precipitate. Single crystals were obtained by slow evaporation of the ethanol (51 mg, 76%). Elemental analysis calcd (%) for $C_{52}H_{81}N_3NiO_3·H_2O$: C 71.55, H 9.58, N 4.81; found: C 71.17, H 9.53, N 4.85; ^{1}H NMR (300 MHz, CD_3OD, 298 K, TMS): δ = 8.7–8.65 (m, 1H), 8.33 (s, 1H), 7.80 (d, ^4J = 2.6 Hz, 1H), 7.7–7.6 (m, 1H), 7.21 (d, ^4J = 2.5 Hz, 1H), 7.11 (d, ^4J = 2.5 Hz, 1H), 7.06 (d, ^4J = 2.6 Hz, 1H), 6.95–6.87 (m, 1H), 6.78–6.71 (m, 1H), 3.21–3.07 (m, 8H), 1.60–1.43 (m, 8H), 1.35 (s, 9H), 1.34 (s, 9H), 1.32–1.22 (m, 8H), 1,20 (s, 9H), 1.19 (s, 9H), 0.87 ppm (t, ^3J = 7.3 Hz, 12H); UV/Vis (CH_2Cl_2): λ_{max} (ε) = 325 nm (10600 $M^{-1}cm^{-1}$), 366 (10400), 427 (9400); IR (neat): $\tilde{\nu}$ = 2955, 2896, 2864 w (ν_{CH}), 1594 s ($\nu_{C=O}$), and 1561, 1521 ($\nu_{C=N}$) cm^{-1}. MS: *m/z* (%): 611 (100) [Ni(L^2)]$^-$.

[Ni(L^3)](Bu$_4$N)$_2$: *n*Bu$_4$NOH (360 μL of a 1 M solution in methanol, 360 μmol) was added to a solution of H_4L^3 (50 mg, 87 μmol) and Ni(OAc)$_2$·4H$_2$O (26 mg, 104 μmol) in DMF (5 mL), and the reaction mixture was stirred at 80 °C for four hours. The DMF was then distilled off in vacuo and the raw product was purified over LH 20 (15 g) with methanol as eluent. After evaporation of the solvent, [Ni(L^3)](Bu$_4$N)$_2$ was obtained as a red powder (47 mg, 48%). Single crystals were obtained by slow evaporation of a diethyl ether/pentane solution. Elemental analysis calcd (%) for $C_{68}H_{116}N_4NiO_4·2H_2O$: C 71.12, H 10.53, N 4.88, Ni 5.11; found: C 72.08, H 10.53, N 4.88, Ni 4.97. ^{1}H NMR (300 MHz, CD_2Cl_2, 298 K, TMS): δ = 8.48 (dd, ^3J = 6.2, ^4J = 3.6 Hz, 2H), 7.77 (d, ^4J = 2.8 Hz, 2H), 6.69 (d, ^4J = 2.8 Hz, 2H), 6.43 (dd, ^3J = 6.2, ^4J = 3.6 Hz, 2H), 3.25–3.19 (m, 16H), 1.42–1.21 (m, 34H), 1,18 (s, 18H), 1.06–1.00 (m, 16H), 0.68 ppm (t, ^3J = 7.2 Hz, 24H). UV/Vis (CH_2Cl_2): λ_{max} (ε) = 341 nm (13300 $M^{-1}cm^{-1}$), 368 (14500), 391 sh (11400) 515 (600). IR (neat): $\tilde{\nu}$ = 2951, 2871 w (ν_{CH}) and 1604 s ($\nu_{C=O}$) cm^{-1}; MS: *m/z* (%): 869 (100) [{Ni(L^3)}(Bu$_4$N)]$^-$, 627 (51) [{Ni(L^3)}H]$^-$, 313 [Ni(L^3)]$^{2-}$.

[1] J. Stubbe, W. A. van der Donk, *Chem. Rev.* **1998**, *98*, 705–762; M. Fontecave, J.-L. Pierre, *C. R. Acad. Sci. Paris Chimie* **2001**, *4*, 531–538; W. Kaim, *Dalton Trans.* **2003**, 761–768.

[2] B. A. Jazdzewski, W. B. Tolman, *Coord. Chem. Rev.* **2000**, 200–202, 633–685; S. Itoh, M. Taki, S. Fukuzumi, *Coord. Chem. Rev.* **2000**, *198*, 3–20; P. Chaudhuri, K. Wieghardt, *Prog. Inorg. Chem.* **2001**, *50*, 151–216, and references therein.

[3] F. Thomas, G. Gellon, I. Gautier-Luneau, E. Saint-Aman, J.-L. Pierre, *Angew. Chem.* **2002**, *114*, 3173–3176; *Angew. Chem. Int. Ed.* **2002**, *41*, 3047–3050; A. Philibert, F. Thomas, C. Philouze, S. Hamman, E. Saint-Aman, J.-L. Pierre, *Chem. Eur. J.* **2003**, *9*, 3803–3812; F. Michel, F. Thomas, S. Hamman, E. Saint-Aman, J.-L. Pierre, *Chem. Eur. J.* **2004**, *10*, 4115–4125; F. Michel, S. Torelli, F. Thomas, C. Duboc, C. Philouze, C. Belle, S. Hamman, E. Saint-Aman, J.-L. Pierre, *Angew. Chem.* **2005**, *117*, 442–445; *Angew. Chem. Int. Ed.* **2005**, *44*, 438–441.

[4] E. Saint-Aman, S. Ménage, J. L. Pierre, E. Defrancq, G. Gellon, *New J. Chem.* **1998**, *22*, 393–394.

[5] F. Thomas, O. Jarjayes, C. Duboc, C. Philouze, E. Saint-Aman, J.-L. Pierre, *Dalton Trans.* **2004**, 2662–2669.

[6] C. G. Pierpont, R. M. Buchanan, *Coord. Chem. Rev.* **1981**, *38*, 45–87; C. G. Pierpont, C. W. Lange, *Prog. Inorg. Chem.* **1994**, *41*, 331–442; C. G. Pierpont, *Coord. Chem. Rev.* **2001**, *216–217*, 99–125.

[7] A. Ghosh, T. Wondimagegn, E. Gonzalez, I. Halvorsen, D. Dolphin, T. Niem, R. H. Felton, I. Fujita, *J. Am. Chem. Soc.* **1975**, *97*, 5288–5290; D. Chang, T. Malinski, A. Ulman, K. M. Kadish, *Inorg. Chem.* **1984**, *23*, 817–824; K. Dongho, L. A. Miller, T. G. Spiro, *Inorg. Chem.* **1986**, *25*, 2468–2470; P. A. Connick, K. A. Macor, *Inorg. Chem.* **1991**, *30*, 4654–4663; J. Seth, V. Palaniappan, D. F. Bocian, *Inorg. Chem.* **1995**, *34*, 2201–2206; M. W. Renner, J. Fajer, *J. Biol. Inorg. Chem.* **2001**, *6*, 823–830.

[8] O. Kahn, J. P. Launay, *Chemtronics* **1988**, *3*, 140–151; P. Gütlich, Y. Garcia, T. Woike, *Coord. Chem. Rev.* **2001**, *219–221*, 839–879.

[9] H. Ohtsu, K. Tanaka, *Angew. Chem.* **2004**, *116*, 6461–6463; *Angew. Chem. Int. Ed.* **2004**, *43*, 6301–6303; H. Ohtsu, K. Tanaka, *Chem. Eur. J.* **2005**, *11*, 3420–3426.

[10] [Cu(L^1)] is the copper(II) complex of H_2L^1 obtained by mixing Cu(ClO$_4$)$_2$·6H$_2$O and the ligand in ethanol in the presence of NEt$_3$.[5]

[11] A. Böttcher, H. Elias, E.-G. Jäger, H. Langfelderova, M. Mazur, L. Müller, H. Paulus, P. Pelikan, M. Rudolph, M. Valko, *Inorg. Chem.* **1993**, *32*, 4131–4138.

[12] H. M. Chang, H. H. Jaffe, *Chem. Phys. Lett.* **1973**, *23*, 146–148; H. M. Chang, H. H. Jaffe, C. A. Masmandis, *J. Phys. Chem.* **1975**, *79*, 1118–1129; J. Takahashi, T. Shida, *Bull. Chem. Soc. Jpn.* **1994**, *67*, 2038–2046; J. Takahashi, T. Momose, T. Shida, *Bull. Chem. Soc. Jpn.* **1994**, *67*, 964–977; L. J. Johnston, N. Mathivanan, F. Negri, W. Siebrand, F. Zerbetto, *Can. J. Chem.* **1993**, *71*, 1655–1662; R. Liu, K. Morokuma, A. M. Mebel, M. C. Lin, *J. Phys. Chem.* **1996**, *100*, 9314–9322; J. G. Radziszewski, M. Gil, A. Gorski, J. Spanget-Larsen, J. Waluk, B. J. Mroz, *J. Chem. Phys.* **2001**, *115*, 9733–9738.

[13] [Zn(L^1)] is the zinc(II) complex of H_2L^1 obtained by mixing Zn(ClO$_4$)$_2$·6H$_2$O and the ligand in ethanol in the presence of NEt$_3$. The phenoxylzinc radical species [Zn(L^1)]$^+$ exhibits an unresolved isotropic (S = 1/2) signal at g_{iso} = 2.005 at 260 K. [Zn(L^1)]$^{2+}$ is a diradical species where the two spins are antiferromagnetically exchange-coupled (J estimated to be about −13 cm^{-1}); O. Rotthaus, O. Jarjayes, F. Thomas, C. Philouze, E. Saint-Aman, J.-L. Pierre, unpublished results.

[14] R. S. Drago, E. I. Baucom, *Inorg. Chem.* **1972**, *11*, 2064–2069; F. V. Lovecchio, E. S. Gore, D. H. Busch, *J. Am. Chem. Soc.* **1974**, *96*, 3109–3118; H. J. Krüger, R. H. Holm, *Inorg. Chem.* **1987**, *26*, 3645–3647; P. A. Connick, K. A. Macor, *Inorg. Chem.* **1991**, *30*, 4654; T. J. Collins, T. R. Nichols, E. S. Uffelman, *J. Am. Chem. Soc.* **1991**, *113*, 4708–4709; F. Azevedo, M. A. Carrondo, B. Castro, M. Convery, D. Domingues, C. Freire, M. T. Duarte, K. Nielsen, I. C. Santos, *Inorg. Chim. Acta* **1994**, *219*, 43–54; D. Pinho, P. Gomes, C. Freire, B. De Castro, *Eur. J. Inorg. Chem.* **2001**, 1483–1493; Z. Xiao, B. O. Patrick, D. Dolphin, *Inorg. Chem.* **2003**, *42*, 8125–8127.

[15] A similar experiment performed in CH_3NO_2 revealed a behavior that is quite similar to that in CH_2Cl_2. The T_C is, however, shifted to 240 K, a value corresponding to the melting point of the mixture CH_3NO_2 + 0.1 M TBAP.

[16] Y. Shimazaki, F. Tani, K. Fului, Y. Naruta, O. Yamauchi, *J. Am. Chem. Soc.* **2003**, *125*, 10512–10513.

[17] This may be interpreted in different ways, such as fast relaxation, changes in electronic distribution, or dimerization. We tend to favor the former hypothesis since a similar behavior (EPR silence at 298 K) is observed for the pyridine adducts [Ni(L^2)(Py)$_2$] and [Ni(L^3)(Py)$_2$]$^-$.

[18] J. Müller, A. Kikuchi, E. Bill, T. Weyhermüller, P. Hildebrandt, L. Ould-Moussa, K. Wieghardt, *Inorg. Chim. Acta* **2000**, *297*, 265–277; Y. Shimazaki, S. Huth, S. Karasawa, S. Hirota, Y. Naruta, O. Yamauchi, *Inorg. Chem.* **2004**, *43*, 7816–7822.

[19] A. Aukauloo, X. Ottenwaelder, R. Ruiz, S. Poussereau, Y. Pei, Y. Journaux, P. Fleurat, F. Volatron, B. Cervera, M. C. Muñoz, *Eur. J. Inorg. Chem.* **1999**, 1067–1071; D. Herebian, E. Bothe, E. Bill, T. Weyhermüller, K. Wieghardt, *J. Am. Chem. Soc.* **2001**, *123*, 10012–10023; C.-H. Sieh, I.-J. Hsu, C.-H. Lee, S.-C. Ke, T.-Y. Wang, G.-H. Lee, Y. Wang, J.-M. Chen, J.-F. Lee, W. F. Lians, *Inorg. Chem.* **2003**, *42*, 3925–3933; X. Ottenwaelder, R. Ruiz-Garcia, G. Blondin, R. Carasco, J. Cano, D. Lexa, Y. Journaux, A. Aukauloo, *Chem. Commun.* **2004**, 504–505; S. Blanchard, F. Neese, E. Bothe, E. Bill, T. Weyhermüller, K. Wieghardt, *Inorg. Chem.* **2005**, *44*, 3636–3656.

[20] The pyridine adduct of **2** decomposes significantly during the experiment, thus precluding any determination of logβ. The logβ values (M^{-2}) for Equation (1) as a function of T are: for **1**$^+$: 6.71 ± 0.09 (298 K), 7.94 ± 0.14 (263 K), and 8.76 ± 0.18 (243 K); for **2**: 7.26 ±

0.13 (233 K); for $\mathbf{3}^-$: 2.41 ± 0.06 (298 K), 4.04 ± 0.09 (263 K), and 5.43 ± 0.10 (238 K). The parameters $\Delta H^{\neq}$ and $\Delta S^{\neq}$ could be obtained from these values: $\Delta H^{\neq} = 51.7\ \mathrm{kJ\,mol^{-1}}$ and $\Delta S^{\neq} = -44.9\ \mathrm{J\,mol\,K^{-1}}$ for $\mathbf{1}^+$ and $\Delta H^{\neq} = 68.2\ \mathrm{kJ\,mol^{-1}}$ and $\Delta S^{\neq} = -183\ \mathrm{J\,mol\,K^{-1}}$ for $\mathbf{3}^-$.

[21] T. J. Collins, T. R. Nichols, E. S. Uffelman, *J. Am. Chem. Soc.* **1991**, *113*, 4708–4709.

[22] Owing to the confidence level of ±0.05 mT on A_x and A_y, the unpaired spin density on the pyridine ^{14}N could not be calculated accurately. In the 1:1 $[Ni(L^1)]^+$:pyridine mixture we were able to trap the 1:1 pyridine adduct, which is characterized by a triplet (instead of a quintuplet) in the low-field component. As expected, the A_{zz} value (2.5 mT) of $[Ni(L^1)(Py)]^+$ is higher than that of $[Ni(L^1)(Py)_2]^+$. From the UV/Vis titration, a $\log\beta$ value of 4.15 ± 0.05 was obtained at 298 K for the equilibrium $[Ni(L^1)]^+ + Py \rightleftarrows [Ni(L^1)(Py)]^+$.

[23] B. De Castro, C. Freire, *Inorg. Chem.* **1990**, *29*, 5113–5119; C. Freire, B. De Castro, *J. Chem. Soc. Dalton Trans.* **1998**, 1491–1498; I. C. Santos, M. Vilas-Boas, M. F. M. Piedade, C. Freire, M. T. Duarte, B. de Castro, *Polyhedron*, **2000**, *19*, 655–664.

[24] The two-electron-oxidized species $\mathbf{1}^{2+}$ and **3** were generated electrochemically (the cations $\mathbf{2}^+$ and $\mathbf{3}^+$ were too unstable to be generated electrochemically). However, the low stability of their pyridine adducts, and the lack of X-band EPR signals, makes the assignment of the oxidation locus difficult (see Supporting Information).

[25] J. Wöltinger, J. E. Bäckvall, A. Zsigmond, *Chem. Eur. J.* **1999**, *5*, 1460–1467.

[26] M.-A. Muñoz-Hernándes, T. S. Keizer, S. Parkin, B. Patrick, D. A. Atwood, *Organometallics* **2000**, *19*, 4416–4421.

Received: July 29, 2005
Revised: September 28, 2005
Published online: December 21, 2005

